

Article

Deformation Mechanism and Stability Control of Roadway Surrounding Rock with Compound Roof: Research and Applications

Yang Yu ^{1,*}, Xiangyu Wang ², Jianbiao Bai ³, Lianying Zhang ¹ and Hongchun Xia ¹

¹ College of Civil Engineering, Xuzhou University of Technology, Xuzhou 221111, China; zhanglianying@xzit.edu.cn (L.Z.); xiahongchun@xzit.edu.cn (H.X.)

² School of Mines, China University of Mining & Technology, Xuzhou 221116, China; wangxiangyu79@cumt.edu.cn

³ State Key Laboratory of Coal Resources & Safe Mining, China University of Mining & Technology, Xuzhou 221116, China; glorycumt@cumt.edu.cn

* Correspondence: yuyang@xzit.edu.cn; Tel.: +86-0516-83689920

Received: 13 February 2020; Accepted: 12 March 2020; Published: 14 March 2020



Abstract: In view of problems with roadways with a compound roof, such as the occurrence of instability in the roof strata, ease of separation of the layer caving, difficulty of maintenance, and poor safety, we established a mechanical calculation model of a roadway with compound roof using the elastic mechanics theory, taking the stability control of a roadway with compound roof at a coal mine in Guizhou Province, China as the research background, and based on the actual characteristics of the coal seam and the roof and floor slate. Expressions of the separation layer and instability limit load of compound roof were derived, and the calculation and verification were carried out in combination with the actual conditions. By means of numerical simulation, the distribution and evolution laws of stress, displacement and plastic zone of roadways with a compound roof were studied, and the deformation characteristics and instability mechanism of roadways with a compound roof were revealed: (1) in early stage deformation of roadway, the amount is large, the speed is fast, and the scale is wide; (2) compound roofs are vulnerable to abscission and instability, the bearing capacity of the two sides is low due to softness and cracking, the shear failure of side angles and vertex angles weakens the strength of surrounding rock, and the self-bearing capacity of surrounding rock is low; (3) the bolt and anchor bear relatively large tensile force, and the support structure is easy to be broken up. On this basis, the stability control principle of a roadway with compound roof tunnel was put forward: fast and timely support; high-strength bolt strong support; improving the stability of the roof and the bearing capacity of the two sides; restraining the shear failure of the key bearing parts such as the side angles and the bottom angles, and targeted stability control technology for roadways with a compound roof was developed. The field industrial test showed that the deformation of this roadway with a compound roof was effectively controlled and the overall stability of the roadway was effectively improved. The results of this study could provide useful reference for a roadway with a compound roof under similar conditions.

Keywords: compound roof; roadway; mechanical model; numerical simulation; instability mechanism; stability control

1. Introduction

Among mine accidents in China, roadway roof accidents account for the majority, while among roadway roof accidents, those involving a compound roof are the most severe. A compound roof, also called an abscission roof, is a kind of immediate roof specially combined with special lithology and

mechanical characteristics. Generally, it is a kind of rock of interval distribution with soft rock and hard rock, coal leads, and weak intercalation. The thickness and cohesive force between its layers are relatively small [1–6]. The roof of a compound roof roadway is prone to abscission and subsidence, while both sides are loose coal, therefore, under the pressure of the overlying strata, the interaction between the compound roof and the two sides makes the condition of the surrounding rock worsen, which will lead to instability and even the collapse of the roadway. According to incomplete statistics, over 30% of coal layer roadways in China have compound roofs and this percentage is increasing with the increase of mining depth [7–10]. The maintenance of roadways with compound roofs has become a choke point for mines in China to extend to deeper areas.

Based on this, many scholars have carried out fruitful research. Bai, et al. [11–13] proposed the interaction mechanism between the compound roof and the two sides, revealed the influence of increasing the support strength of the two sides on the compound roof, and pointed out that the two sides and the compound roof should be considered as a whole for support. Wang, et al. [14–16] used theoretical analysis methods to analyze the stress and deformation characteristics of the thick layer compound roof from two aspects of vertical and horizontal stress, and revealed the influence of high horizontal stress on the bending, deformation, and the interlayer delamination of a thick layer compound roof. Li et al. [17–20] studied the compound roof of a roadway driving along the goaf of a mine, and proposed the use of reinforced support methods, such as high pre-stress anchors, bolts, and shotcrete to control the deformation of the compound roof, as well as verifying its effectiveness. Zhang et al. [21–23] proposed the characteristics of the plastids that are unique to the compound roof, and comprehensively judged whether the compound roof is separated, based on whether the layer on the compound roof turned into a load being exerted on the lower layer load, the limit span, and the flexural deformation of each layer of the compound roof. Wu et al. [24–27] put forward the criteria and basis for judging separation stability, through five levels and six orthogonal factors including original rock stress, roadway width, compound roof lithology, compound roof thickness, structural cohesion, and structural internal friction angle that affect the separation of the compound roof. He et al. [28–31] analyzed the characteristics of a jointed compound roof, pointed out its deformation mechanics mechanism with dual attributes of expansion type and structural deformation type, studied the transformation process from composite to a single mechanical mechanism, and put forward the form and sequence of combined support with bolt, mesh, and cable. However, the various layers of the compound roof were prone to plastic shear movement along the sliding surface, and then flexed and deformed to leave the layer. The self-stability of the compound was poor and the support was difficult. Scholars have studied the instability mechanism and pre-stress control of coal roofs in compound roofs, focusing more on the mechanical properties and deformation mechanisms of the compound roof, while research on the instability mechanisms of a compound roof under the influence of multiple weak faces is rarely involved. In addition, further research on the response law of pre-stress diffusion to multiple weak surfaces is very necessary.

Therefore, in order to solve the universal problem of the control of a roadway with a compound roof, taking a coal mine in Guizhou province in China as the background, the abscission instability of the compound roof, the deformation mechanism of the roadway surrounding rock, and stability control were researched, and ways to control the deformation and collapse of a roadway with a compound roof was explored. This work is beneficial in furthering the excavation and support process for complex and difficult roadways, which is of important theoretical value and practical significance.

2. Engineering Geological Condition

A mine in Guizhou province in China mines coal seam 6#, the structure of which is simple, with 2.41 m of thickness, a dip angle between 1° and 3° , and a platts hardness coefficient of approximately 0.8, and it is a soft coal seam. The positional relation of roadways is shown in Figure 1. Mining face 1603 is the first mining face in the west of mine field, with an average burial depth of 260 m, strike length of 988 m, and inclined width of 150 m. The transportation roadway of mining face 1603 tunnels along the

floor of coal seam 6#, with the section size: width \times height = 4.3 m \times 2.7 m. Coal seam 6# is the high gas outburst seam, where the gas drainage roadway in the floor of the coal seam is laid in advance to pre-pump gas into the front of the excavation face. By sampling the coal and rock layers near the 1603 mining face, and performing rock mechanics tests on the processed samples in the laboratory, combined with the preliminary geological survey report of the coal mine, the lithology and mechanical parameters of the roof and floor of coal seam 6# were determined, and can be found in Table 1. The surrounding rock of the 1603 mining face has a wide range of loosening zone, large deformation of the surrounding rocks, and different degrees of delamination in the compound roof from the information obtained with early investigations and tests, including instruments such as seismographs, borescopes, and infrared rangefinders. The preliminary survey results are shown in Figure 2.

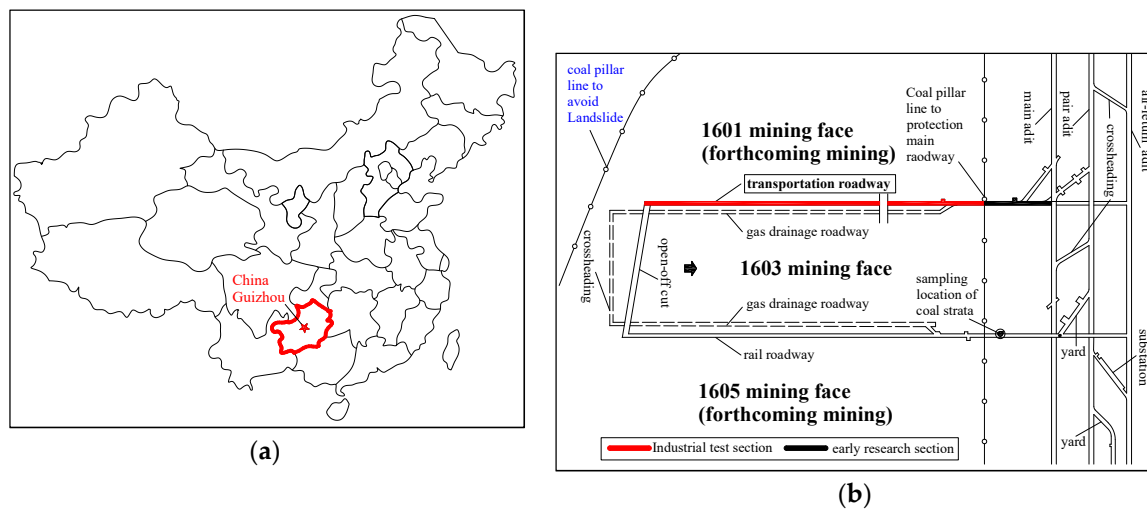


Figure 1. (a) Location of the mine; (b) the location of mining face.

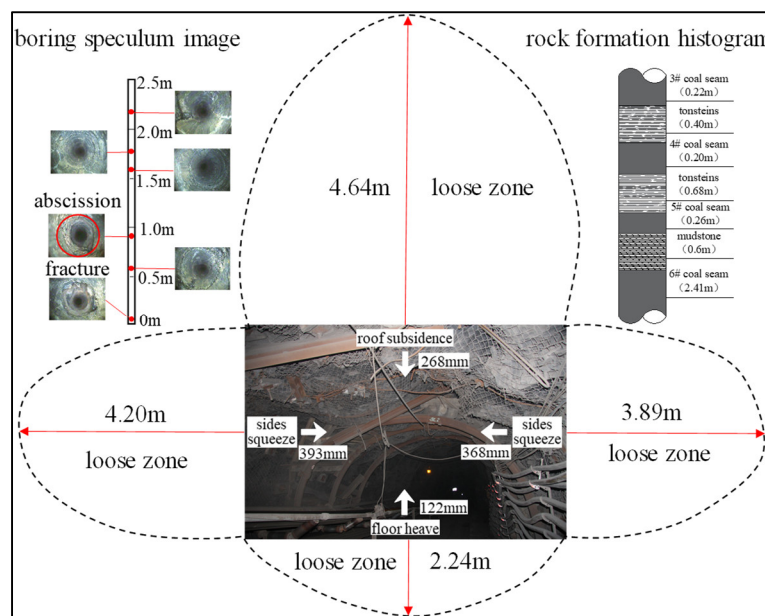


Figure 2. The preliminary survey results.

Table 1. The lithology and mechanical parameters of roof and floor of coal seam 6#.

Location	Lithology	Thick-ness (m)	Elasticity-modulus (MPa)	Poisson Ratio	Compr-essive Strength (MPa)	Cohe-sion (MPa)	Internal Friction Angle (°)	Density (kg·m ⁻³)
Overlying strata	limestone	13.27	7404	0.23	61.40	13.0	44	2730
	argillaceous siltstone	3.30	4038	0.28	24.30	5.3	43	2650
	pack sand	2.30	5857	0.25	36.20	7.7	44	2600
	silty mudstone	6.21	3166	0.30	19.10	4.3	42	2630
	limestone	1.38	7404	0.23	61.40	13.0	44	2730
Main roof	argillaceous siltstone	2.09	4038	0.28	24.30	5.3	43	2650
Compound roof	3# coal seam	0.22	445	0.33	6.25	2.0	25	1530
	tonsteins 2	0.40	1938	0.32	10.80	2.5	40	2620
	4# coal seam	0.20	445	0.33	6.25	2.0	25	1530
	tonsteins 1	0.68	1635	0.32	10.80	2.5	40	2620
	5# coal seam	0.26	445	0.33	6.25	2.0	25	1530
	mudstone	0.60	926	0.32	10.80	2.5	40	2620
Coal seam	6# coal seam	2.41	4038	0.33	6.25	2.0	25	1530
immediate floor	mudstone	1.42	926	0.32	10.80	2.5	40	2620
Main floor	argillaceous siltstone	2.41	4038	0.28	24.30	5.3	43	2650
Under strata	7# coal seam	0.75	227	0.33	6.25	2.0	25	1530
	siltstone	11.31	6598	0.26	30.60	6.7	42.5	2660
	8# coal seam	0.92	227	0.33	6.25	2.0	25	1530
	siltstone	10.42	6598	0.26	30.60	6.7	42.5	2660
	mudstone	8.35	926	0.32	10.80	2.5	40	2620

3. Mechanical Structure Model of Roadway Compound Roof

Under the load of the overlying strata, abscission of different degrees occurs in the compound roof, and the bearing capacity of the compound roof decreases. Given that the length of the roadway is far longer than its width, the compound roof is regarded as infinite plate. As shown in Figure 3, the compound roof consists of m layers of soft rock, which are numbered from n_1 to n_m , the thicknesses of which are from h_1 to h_m , the width and height of the roadway are a and b respectively, and the thickness of compound roof is h . The vertical distributed load borne by the upper part of the strata of the compound roof is q , and horizontal force is P .

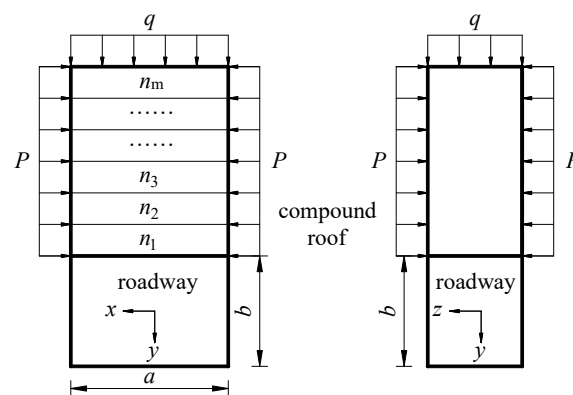


Figure 3. Structural mechanics module.

3.1. Deflection and Stress Distribution of Compound Roof

Under the stress of distributed load q , the elastic surface differential Equation (32) of layer n_1 is as follows:

$$Q_1 \nabla^4 w_1 = q, Q_1 = E_1 h_1^3 / (12(1 - \mu_1^2)), \quad (1)$$

In the equation: w_1 is the deflection of layer n_1 ; Q_1 is the flexural rigidity of layer n_1 ; q is distributed load; E_1 is the elastic modulus of layer n_1 ; h_1 is the thickness of layer n_1 , m ; μ_1 is Poisson ration of layer n_1 .

Generally, q is the function of x , and to facilitate analysis, make q a constant. Use the boundary condition of two edges fixed to solve the deflection expression:

$$w_1 = qa^4(1 - 8x^2/a^2 + 16x_4/a^4)/(384Q_1), \quad (2)$$

When $x = 0$, w_1 achieves a maximum of:

$$w_{1max} = qa^4/(384Q_1), \quad (3)$$

Stress caused by the horizontal force P is represented by the equation:

$$\sigma_x = P/h_1, \sigma_y = \mu_1 P/h_1, \quad (4)$$

Stress of the layer n_1 can be found with:

$$\begin{aligned} \sigma_x &= qza^2(12x^2/a^2 - 1)/2h_1^3 + P/h_1, \sigma_y = qza^2(12x^2/a^2 - 1)/2h_1^3 + \mu_1 P/h_1, \\ \sigma_z &= 2q(1/2 - z/h_1)^2(1 + z/h_1), \tau_{zx} = 6qx(h_1^2/4 - z^2)/h_1^3, \end{aligned} \quad (5)$$

Regard the infinite plate as a thin plate; τ_{xy} and τ_{yz} are both 0.

3.2. Abscission and Instability Conditions of Compound Roof

As for layer n_2 , if the deflection w_2 is less than w_1 , then the deflection expression is as follows:

$$w_2 = qa^4(1 - 8x^2/a^2 + 16x_4/a^4)/(384Q_2), \quad (6)$$

As for layer n_2 , if the deflection w_2 is more than w_1 , then strata n_2 and layer n_1 form compound slab without abscission between them. The elastic modulus and Poisson ration of the compound slab is as follows:

$$E_{12} = (E_1 h_1 + E_2 h_2)/(h_1 + h_2), \mu_{12} = (\mu_1 h_1 + \mu_2 h_2)/(h_1 + h_2), \quad (7)$$

The deflection expression of the compound slab is:

$$W_{12} = 12qa^4(1 - \mu_{12})(1 - 8x^2/a^2 + 16x_4/a^4)/(384E_{12}h_1^3), \quad (8)$$

The stress is the biggest at the fixed end of strata n_1 , and according to Tresca yield criterion, the shearing strength of layer n_1 is as follows:

$$\tau_1 = |\sigma_x|/2, \quad (9)$$

Make $x = a/2z = h_1/2$, bring them into formula (5), then it draws the critical yield load of layer n_1 :

$$q_0 = (4\tau_1 h_1^2 - 2ph_1)/a^2, \quad (10)$$

3.3. Testifying Example of Compound Roof Abscission

The compound roof of the transportation roadway of mining face 1603 consists of mudstone, the 3#, 4#, and 5# coal seams, and their tonsteins. In order to figure out whether the compound roof abscises, it can be decided successively from the bottom mud rock layer of n_1 to the top. We made the overlying strata load $q = 260 \times 25,000 \text{ Pa} = 6.5 \text{ MPa}$ and the roadway width $a = 4.3 \text{ m}$, and for other parameter details refer to Table 1.

3.3.1. Layer n_1 and Layer n_2

The deflection curve of layer n_1 with mudstone and layer n_2 with the 5# coal seam are shown in Figure 4. As is shown, the deflection of layer n_2 is far greater than that of layer n_1 . Both of them form a compound board to bear together.

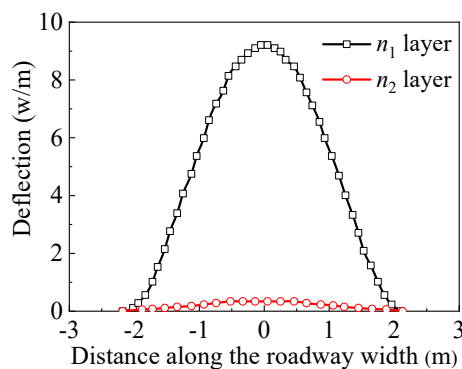


Figure 4. The deflection curve of n_1 and n_2 layers.

3.3.2. Layers n_1 and n_2 Compound Board, and Layer n_3

Layer n_3 is relatively hard mud rock tonsteins. The deflection curves of layers n_1 and n_2 compound board and layer n_3 are shown in Figure 5. The largest deflection of layer n_3 is 142 mm, less than that of the compound board of layer n_1 and n_2 , which is 147 mm. Compound board of layer n_1 and n_2 abscises from layer n_3 , and the largest abscission value is 5 mm. So the completeness of the compound roof is damaged, and the bearing capacity is decreased.

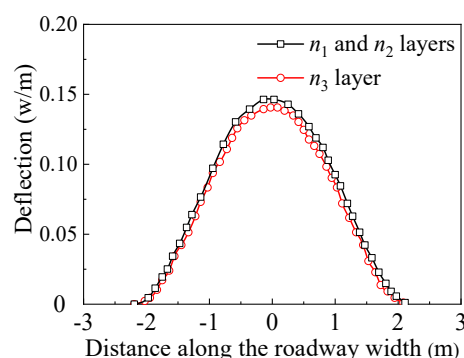


Figure 5. The deflection curve of layers n_1 and n_2 compound board and n_3 layer.

3.3.3. Layer n_3 and Layer n_4

Layer n_4 is 4# coal seam, as the thickness, elasticity modulus and Poisson's ratio of layer n_4 are less than that of layer n_3 . Therefore, there is no abscission between layer n_3 and layers n_4 , and both of them form the compound board.

As is shown in Figure 6, the largest deflection of the compound board that consists of layer n_3 and layer n_4 is only 79 mm, far less than that of the compound board of layer n_1 and n_2 , which is

147 mm. There is abscission between the compound board of layers n_1 and n_2 and the compound board of layers n_3 and n_4 , with the largest abscission of 68 mm. So the completeness of the compound roof is further damaged, and the bearing capacity continues to decrease.

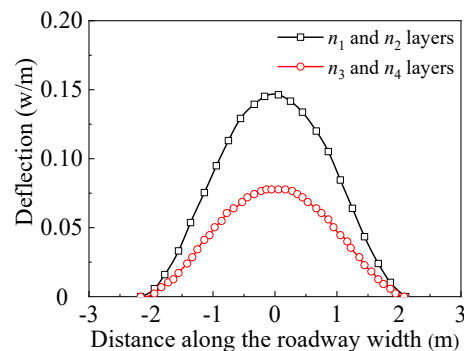


Figure 6. The deflection curve of layers n_1 and n_2 compound board and layers n_3 and n_4 compound board.

3.3.4. Compound Roof of the Compound Board of LAYERS n_3 and n_4 , and Layer n_5

Layer n_5 is tonsteins. As is shown in Figure 7, the largest deflection of layer n_5 is 589 mm, far more than that of the compound board of layers n_3 and n_4 , which is 79 mm. The compound board of layers n_3 and n_4 combines again with layer n_5 to form the compound board with larger thickness. Layer n_6 is the 3# coal layer, and its thickness, elasticity modulus, and Poisson ratio are all less than that of the compound board of layer n_3 and n_4 . What is more, the compound board of layer n_3 and n_4 is strengthened by combining with layer n_5 . Therefore, there is no abscission between layer n_6 and the compound board of layers n_3 , n_4 , and n_5 , and all of them form the new compound board.

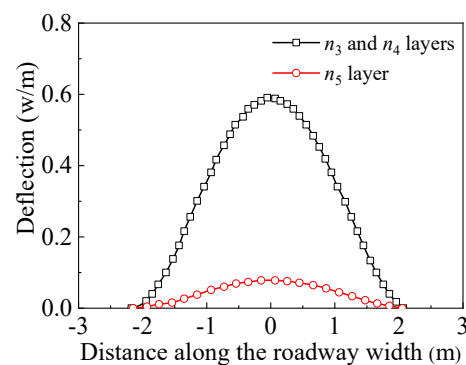


Figure 7. The deflection curve of n_3 and n_4 compound board and n_5 layer

As is shown in Figure 8, the compound roof of the transportation roadway of mining face 1603 consists of two parts, that is, the compound board of layers n_1 and n_2 , and the compound board of layers n_3 , n_4 , n_5 , and n_6 . The abscission occurs between these two compound boards. While regardless of the bulking deformation and distortion of the compound roof, the largest abscission value of the compound roof is 131 mm, which shows that the completeness of the compound roof is largely destroyed, the effective bearing thickness decreases remarkably, and the stability also decreases.

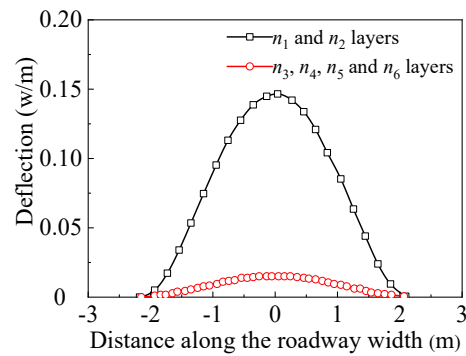


Figure 8. The deflection curve of n_1 and n_2 compound slab and $n_3, n_4, n_5,$ and n_6 compound board.

4. Numerical Simulation of Roadway Compound Roof

4.1. Model

In order to reveal the mechanism of deformation instability, the numerical evolution method was used to study the distribution and evolution law of the surrounding rock stress field, displacement field and plastic area during the excavation and mining of the roadway compound roof under the condition of floor gas drainage roadway disturbance. According to the actual geological conditions, we chose a 100 m section of the transportation roadway of mining face 1603 as the study object, and the size of the model was length \times width \times height = 130 m \times 100 m \times 84 m, with 432800 of total cells and 450585 of total nodes. The sides of the model moved horizontally, and the bottom was not allowed to move vertically. The upper surface of the model is the stress boundary. We exerted a load of 5.75 MPa to simulate the dead weight stress of the overlying strata, and the side pressure coefficient was 1.0. All the materials were consistent with Mohr-Coulomb criterion. The metal net was simulated with a lining structure. The numerical simulation model is shown in Figure 9. The mechanical parameters of relevant rocks refer to Table 1. The numerical simulation was divided into the following steps: (1) excavation of floor gas drainage roadway and timely support, and the calculated value model was balanced; (2) after the completion of step (1), the compound roof roadway was excavated and supported in time, and the calculated value model was balanced.

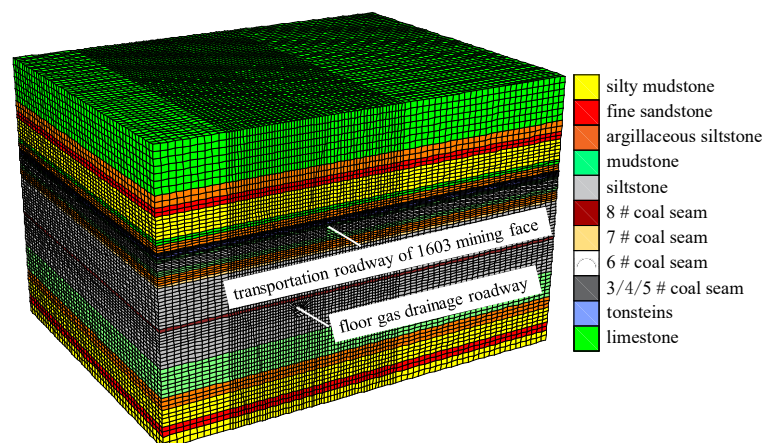


Figure 9. Numerical simulation model.

4.2. Deformation Instability Mechanism of Roadway

After the roadway is excavated, surrounding rock stress will reorient. Shallow surrounding rock deforms lot due to crushing and expansion, and a certain scale of stress concentration area forms in deep surrounding rocks. Through studying the features of stress, deformation, and damage of

the roadway, the deformation mechanism of roadway surrounding rocks with a compound roof can be revealed.

4.2.1. Stress Distribution

(1) The vertical stress of two sides. The vertical stress distribution of two sides is shown in Figure 10. The shallow surrounding rock of two sides within 4 m form stress-decreasing areas due to crushing and expansion deformation, the load of the overlying strata is mainly shouldered by the vertical stress-increasing areas of two sides within the scope of 4 m to 7m, and the vertical stress peak forms at the point 5 m from the two sides, which is about 8.5 MPa, with a stress concentration coefficient of 1.3. The surrounding rock, within the scope of 1 m to 2 m from the front of excavation face, forms a vertical stress-decreasing area, and that within the scope of 2 m to 4 m from the front of the excavation face forms a vertical stress-increasing area.

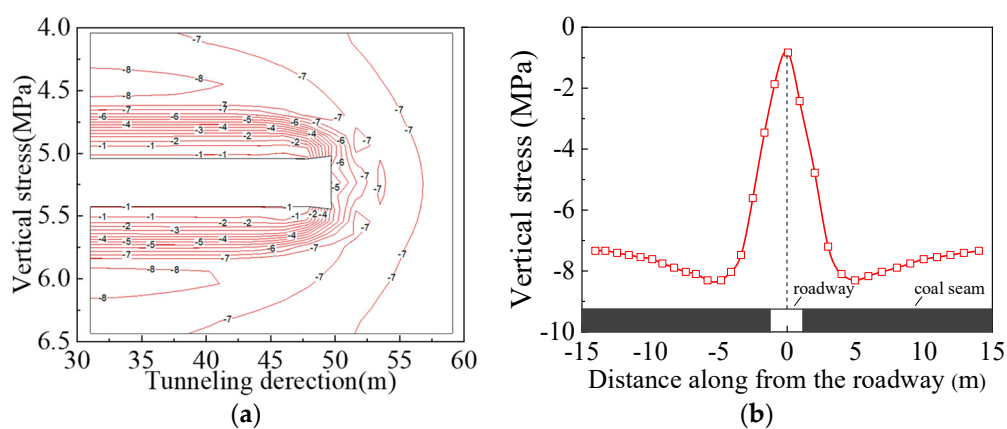


Figure 10. The vertical stress distribution of two sides of the roadway: (a) contour; (b) curve.

(2) Horizontal stress of roof and floor. The distribution of horizontal stress of roof and floor is shown in Figure 11. The shallow surrounding rock within the areas of 4 m above the roof and 2 m below the floor form horizontal stress-decreasing areas, due to crushing and expansion deformation. The surrounding rocks within the scope of 4 m to 7 m above the roof and 2 m to 5 m below the floor form a horizontal stress concentration area. Horizontal stress peaks appear at 6 m above the roof and 3 m below the floor. The horizontal stress peak of the roof is 10.3 MPa and the stress concentration coefficient is 1.6. The horizontal stress peak of the floor is 9.6 MPa and the stress concentration coefficient is 1.5. Further 1 m to 2 m from the front of excavation face, it forms horizontal stress-decreasing area, and 2 m to 4 m from the front of excavation face, it forms horizontal stress-increasing area.

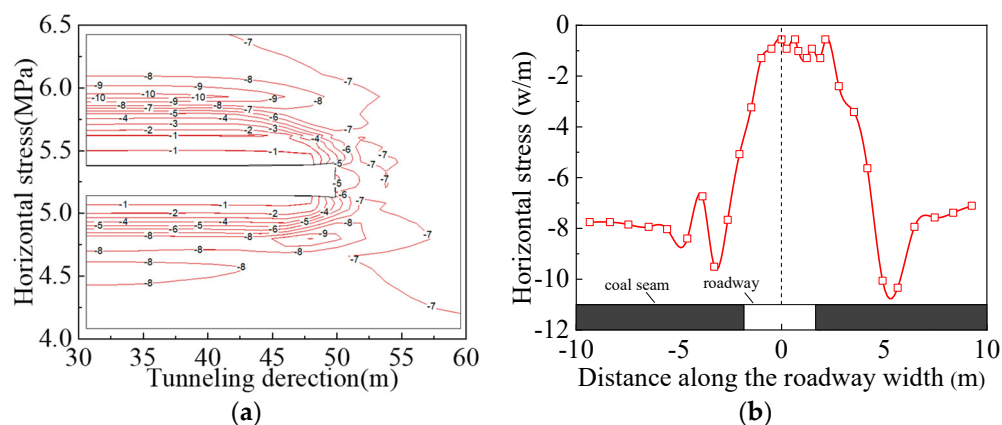


Figure 11. The horizontal stress distribution of the roof and floor of the roadway: (a) contour; (b) curve.

4.2.2. Displacement Distribution

(1) Vertical displacement of roof and floor. Vertical displacement distribution of roof and floor is shown in Figure 12. In front of the excavation face, the vertical displacement of surrounding rock is relatively small. Within the scope of 4 m back from the excavation face, the vertical displacement of roof and floor increase sharply, while beyond 4 m, the deformation basically stabilizes. The largest roof convergence is 240 mm, and the largest floor heave amount is 100 mm. At 10 m deep in the roof, the convergence is still more than 10 mm, and at 10 m deep in the floor, the floor heave amount is still more than 6 mm.

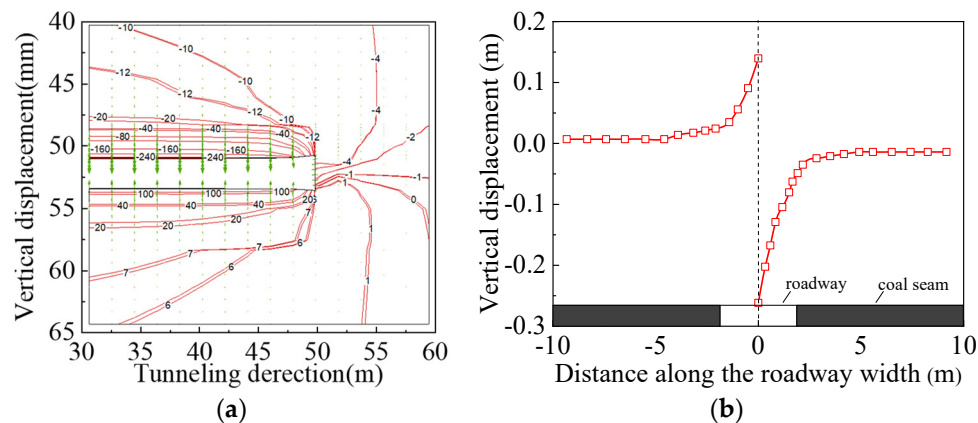


Figure 12. The vertical displacement distribution of the roof and floor of the roadway: (a) contour; (b) curve.

(2) The horizontal displacement of two sides. The horizontal displacement distribution of two sides is shown in Figure 13. In front of the excavation face, the horizontal displacement of surrounding rock is relatively small. Within the scope of 4 m back from the excavation face, the horizontal displacement increase sharply, while beyond 4 m, the deformation stabilizes. The largest deformation of the two sides is 400 mm. At 8 m deep of the two sides, the deformation is still 6 mm.

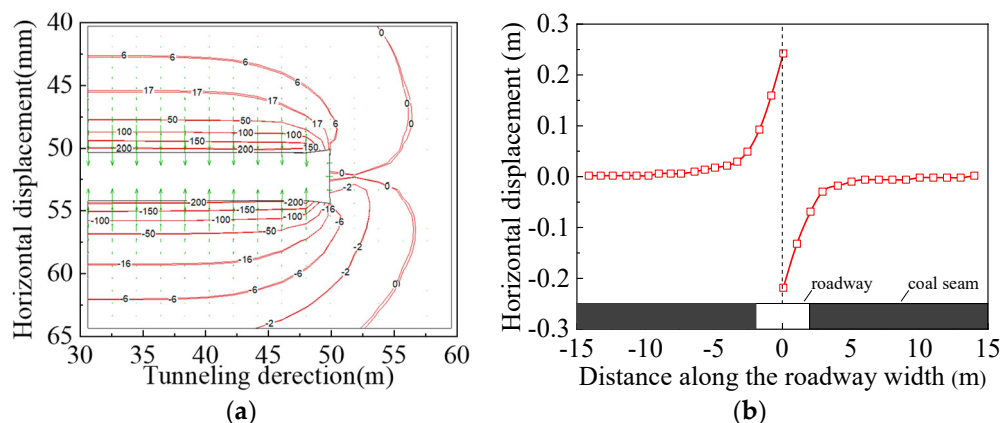


Figure 13. The horizontal displacement distribution of two sides of the roadway: (a) contour; (b) curve.

4.2.3. Plastic Zone Distribution

In front of the excavation face, all of the surrounding rock is subject to shear failure. Within 2 m back from the excavation face, the surrounding rock is mainly subject to combined shear and tensile failure, and this area tends to get unstable. Within 4 m back from the excavation face, the plastic zone extension of the surrounding rock is already stable, and a compound roof tends to abscission and tensile failure. Beyond 4 m back from the excavation face, the compound roof shows the combined

shear and tensile failure, and the deformation of some sections show tensile failure, and stability of the compound roof is low. Side angles and the shallow surrounding rock of sides and floor show the combined shear and tensile failure. The middle shallow surrounding rock of the compound roof shows tensile failure, and the deep surrounding rock shows the combined shear and tensile failure. The plastic zones are shown in Figure 14.

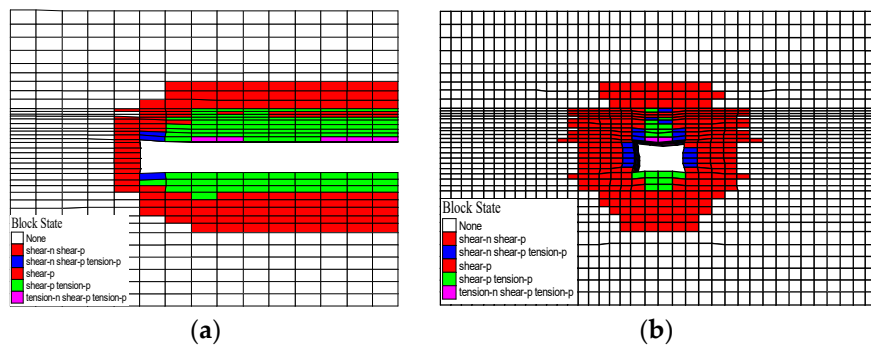


Figure 14. The plastic zone of the roadway. (a) Axial section; (b) Radial section.

4.2.4. Bolt Axial Force

After timely support of the compound roof roadway, the axial force of bolt and anchor is shown in Figure 15. The axial force distribution of a single bolt: the middle part is the largest and both sides are the smallest, and it only bears tensile stress. In the middle of the roof, the axial force of the bolt is the largest, followed by that of the middle of the two sides, and the side angle is the smallest. The largest load of the bolt is 101 kN, and largest load of the anchor is 250 kN. Due to the large abscission and convergence of the compound roof, the bolt and anchor bear a relatively large load.

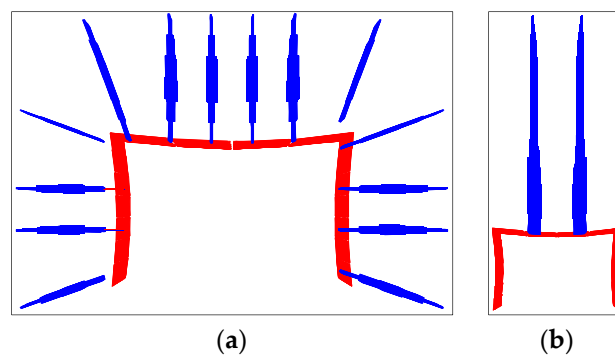


Figure 15. The axial force of the bolt and anchor: (a) bolt; (b) anchor.

5. Stability Control of Surrounding Rock of Compound Roof Roadway

5.1. Principle of Stability Control

The targeted stability control principle is presented with the basis of the deformation instability mechanism of surrounding rock of a compound roof roadway: (1) fast and timely support—control early abscission of compound roof and huge deformation of two sides; (2) strong support with high-strength bolt—increase stability of roof and bearing capacity of the two sides, and control shear failure of key bearing areas such as side angles and floor angles; (3) high pre-stress support—increase support strength, improve the stress of surrounding rock, intensify the strength of surrounding rock, and increase self-bearing capacity of surrounding rock. The principle of stability control is shown in Figure 16.

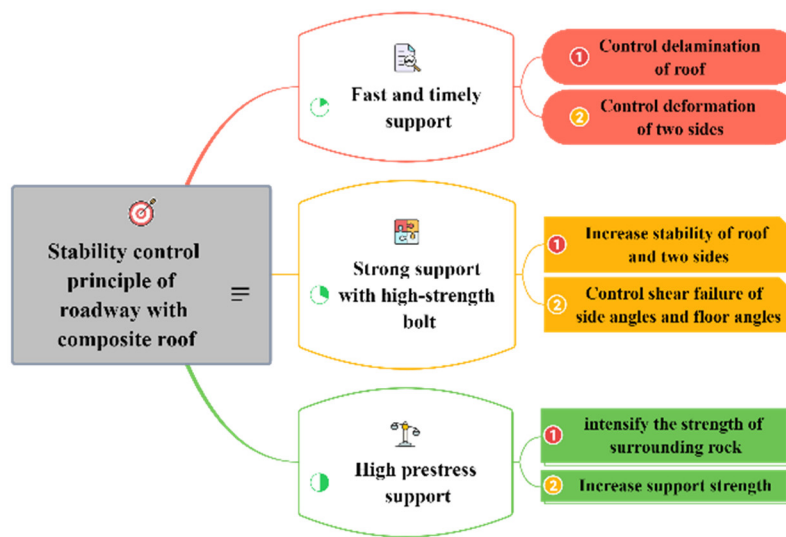


Figure 16. The Principle of stability control.

5.1.1. Fast and Timely Support

Viscoplastic model named power was employed to study the impact of retardation time of support on the stability of the roadway. According to data collected in the field, the back analysis method was used to define the main creep material parameter of the mode, and the parameters were: $A = 3 \times e^{20}$, $n=3$. In the model, the roadway deformation condition is calculated successively when it is timely support, 30 min later, and 60 min later.

As can be seen in Figure 17, when there is timely support, the deformation is best controlled. The roof convergence is 220 mm and the deformation of two sides is 272 mm; 30 min later, the deformation is the most dramatic, the displacement increasing sharply, the roof convergence is 252 mm, and the deformation of two sides is 396 mm; when it is 60 min later, the roof convergence is 258 mm, and the deformation of two sides reaches 402 mm. Therefore, fast and timely support may decrease remarkably the deformation and speed of roadway, which is very effective to control roadway deformation.

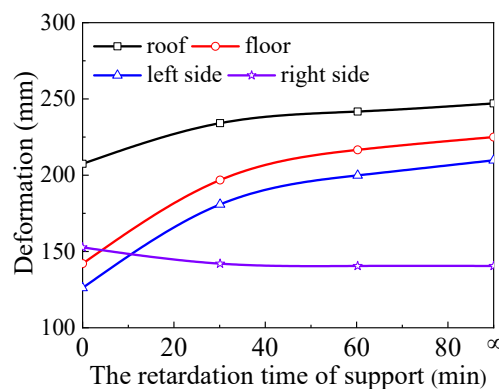


Figure 17. The influence of retardation time to roadway deformation.

5.1.2. Strong Support with High-strength Bolt

All kinds of joints and cracks develop in the compound roof, and they have a large impact on the overall strength of rock. Rock destruction starts from structural plane destruction. Structural plane is the weak link of rock, the weakness of which is enlarged after the roadway is excavated, and rock is vulnerable to shear failure. Bolts may effectively increase shear strength of the structural plane, the function schematic diagram of which is shown in Figure 18.

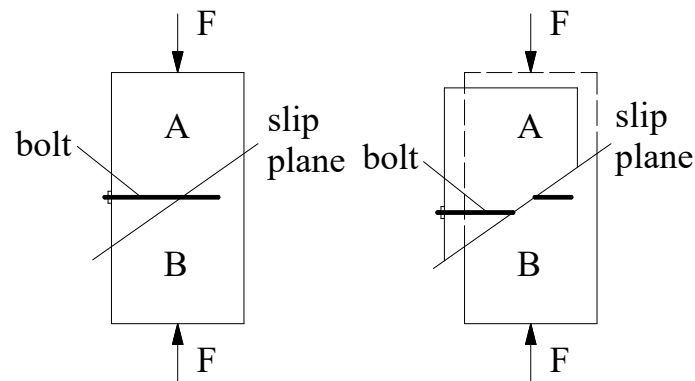


Figure 18. The bolt function schematic diagram.

The joint tangential resistance provided by a bolt is proportionate to the breaking load of the bolt. In Section 3 we can see that the tensile force born by bolt of roadway with compound roof can be as high as 101 kN. For the roadway affected by dynamic pressure, the stress of bolt will be even larger. The diameter of bolt employed in a coal mine is generally between 18 mm and 22 mm. The bolt with texture of BHRB335 and 20 mm of diameter and over 150 kN of breaking load could meet the support requirements of a roadway with a compound roof.

5.1.3. High Pre-stress Support

Related studies show that the larger the confining pressure is, the higher the rock strength is. Before the surrounding rock is damaged, the increase of rock strength exerted by confining pressure is weak. However, after the surrounding rock is damaged, the residual strength of rock is sensitive to the confining pressure. Even a small increase of confining pressure may remarkably increase the residual strength of rock, thus improving the mechanical property of surrounding rock. Study of vertical stress distribution law of surrounding rock under different pre-stress reveals the interaction mechanism between a bolt with high pre-stress and the surrounding rock.

As can be seen in Figure 19, the distribution law of pre-stress at the roof is: (1) stress concentration appears clearly at the tail of the bolt, as it moves far away from the tail, compression stress gradually decreases, and a small area of tensile force appears at the end of the bolt; (2) the effective compression stress area between two bolts is relatively small, but they can form effective compression stress belt when they are combined as a whole, compression pressure near bolt at the two vertex angles of the roadway is the lowest, and compression pressure near the bolt at the middle part of the roof is the highest; and (3) with the increase of pre-stress, the effective compression pressure of the roof extends correspondingly. When the pressure reaches 40 kN, the effective compression pressure zone will not expand, but the maximum pressure of the roof will still be increasing. Given the limitations of construction equipment, the proper pressure of the bolt should be 40–50 kN.

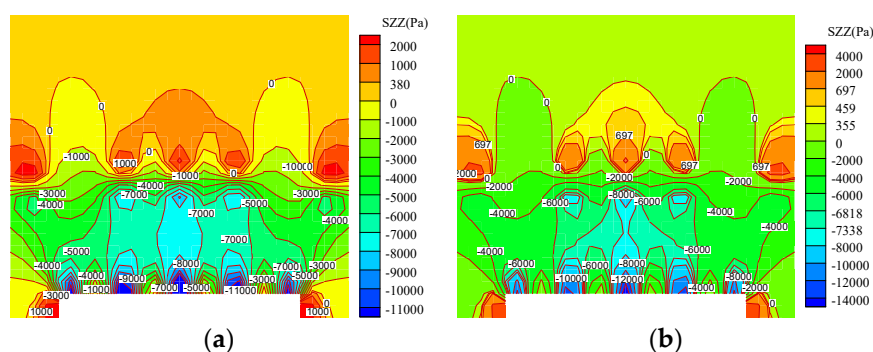


Figure 19. Cont.

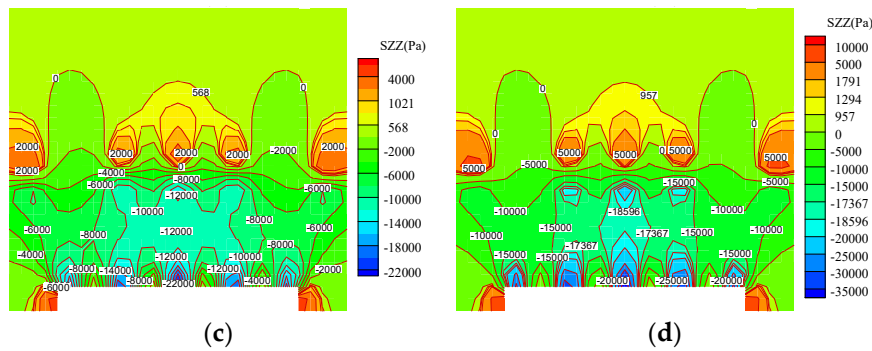


Figure 19. The influence of pre-stress on stress distribution of roof: (a) 20 kN; (b) 40 kN; (c) 60 kN; (d) 80 kN.

5.2. Stability Control Technology

Base on the construction geological conditions, several schemes with reasonable technologies were preliminary selected, and the control effect of various schemes on the deformation of the roadway was analyzed with nonlinear finite difference software FLAC3D. Guided by the principle of “effectiveness, low cost, and fast construction”, the bolt support parameters of roadway at mining face 1603 were defined. The parameters were as follows:

(1) Bolt. The roadway roof and the two sides both employ high-strength thread steel bolt of BHRB335, L2400 mm, $\Phi 20$ mm, the inter-row space of anchor rods is 800 mm \times 800 mm, and the anchor agent employs a CK2340 and a Z2360.

(2) Anchor. The roof employs two anchors with seven steel strands with the type of L7300 mm, $\Phi 17.8$ mm. The inter-row space of anchor is 1600 mm \times 2400 mm, and the anchor agent employs a CK2340 and a Z2360.

(3) Other accessories. The whole section of the roadway is laid with diamond metal net made of iron wire 8#, and $\Phi 14$ mm steel ladder beam is used to integrate bolt. Bolt and anchor both use manganese steel pallet and the specifications are: length \times width \times thickness = 150 mm \times 150 mm \times 10 mm, and length \times width \times thickness = 300 mm \times 300 mm \times 16 mm respectively.

(4) Synchronous and timely support of roof and the two sides is required on construction site; the prestress of bolt and anchor are not less than 50 kN and 120 kN respectively, and the anchorage force of bolt and anchor are not less than 100 kN and 200 kN. The roadway support section is shown in Figure 20.

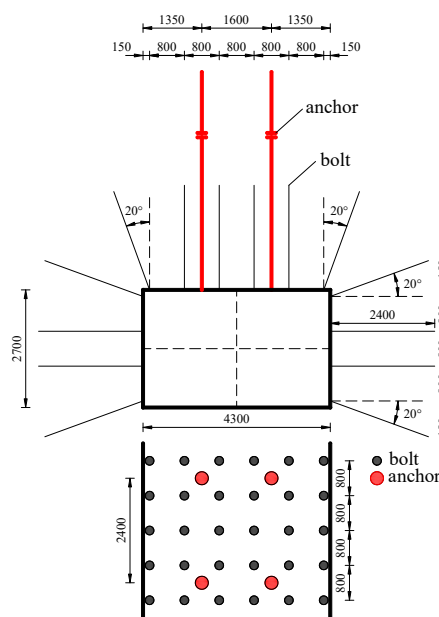


Figure 20. The roadway support section.

5.3. Control Effect of Roadway Surrounding Rock

(1) Roadway displacement monitoring. Fifteen days after the roadway was excavated, the deformation gained speed, and the average deformation rate of the roof and floor rock and the two sides were respectively 8.3 mm/d and 11.3 mm/d. Twenty four days later, deformation tended to stabilize; afterwards, the deformation rate kept decreasing, and the accumulative deformation amount of the roof and floor rock and the two sides were respectively 143 mm and 203 mm. The monitoring curves are shown in Figure 21.

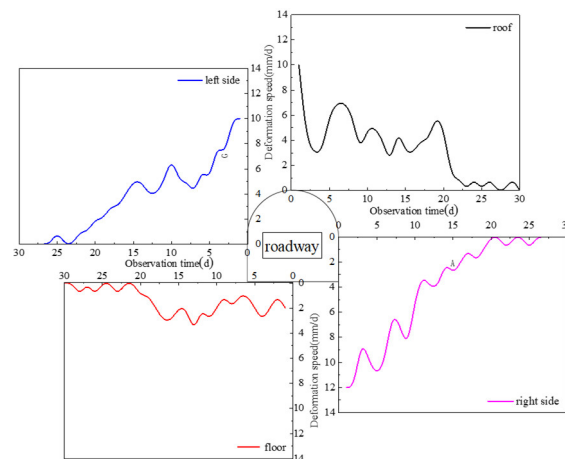


Figure 21. The displacement monitoring curves of roadway surface.

(2) Monitoring of deep surrounding rock displacement. In the anchorage zone that is within 2 m away from the roof, the largest abscission was 25 mm. The stress of the bolt was relatively large, but the maximum abscission was far less than the ultimate strain of the bolt; within the area that is from 2 m to 3 m away from the roof, the surrounding rock activities were intense, and the maximum abscission was 16 mm; within the area that is from 4 m to 5 m away from the roof, disparity of surrounding rock activities was the largest. The maximum abscission was 24 mm, but far less than the reference value of limit abscission of the roof, and the roof is relatively safe. The monitoring curves are shown in Figure 22.

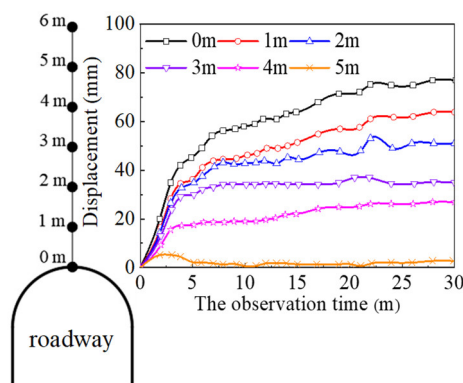


Figure 22. The displacement monitoring curves of deep surrounding rock.

(3) Axial force of bolt and anchor. Bolt stress of the middle part of the roof was the highest, followed by that of the side angles, and that of the vertex angles was the lowest. Twenty four days after the roadway was excavated, the axial force of the bolt tended to stabilize, and the maximum stress of bolt is 127 kN, less than the breaking stress of 150 kN; twenty two days after the roadway was excavated, the axial force of anchor was basically stable. The maximum axial force of the anchor was

185 kN, less than the breaking stress of 300 kN. There is still a large carrier space for bolt and anchor, and the safety factor of the roadway is high. The monitoring curves are shown in Figure 23.

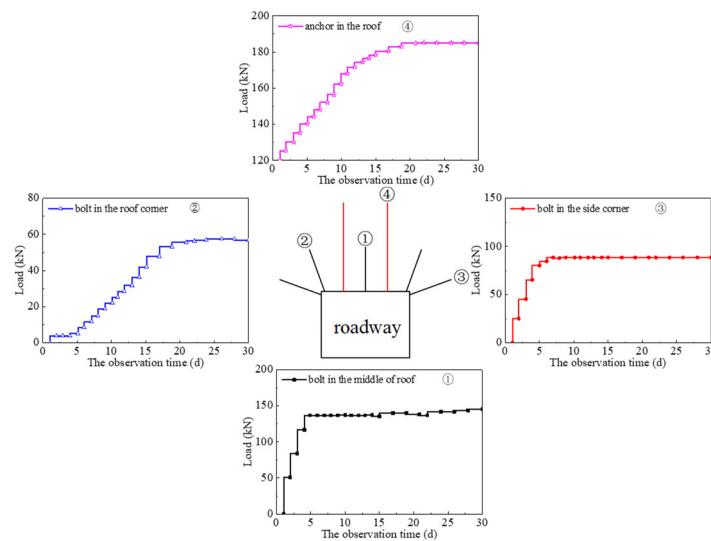


Figure 23. The resistance monitoring curves of bolt and anchor.

6. Discussion

Aiming to help solve the actual tunneling and support problems in a certain coal mine, based on the data and experience obtained from field surveys in underground mines, an elastic mechanics theory was used to establish a compound roof mechanical structure model, and the theoretical calculation results were used to determine the compound roof separation layer. The conclusions are basically consistent with the imaging results of drilling peep, which indicates that the theoretical model can explain the phenomenon of roadway instability under specific conditions, but the universal applicability of the theoretical calculation model needs to be tested. The actual conditions of an underground coal seam are complex, and there are a large number of joints and fissure structures in the interior. The stability of the composite roof is seriously affected by these structures. This is a problem ignored by the calculation model. In follow-up studies the relevant theories of fracture mechanics and damage mechanics should be further considered, and the influence of joint crack structure on the deformation and failure of compound roofs should be researched in depth.

In addition, combining the rock mechanics test of coal and rock sample and the data of mine geological exploration report, the rock mechanics parameters for numerical calculation were preliminarily determined, a numerical simulation model was established that met the actual conditions as much as possible, and the comparison with the actual deformation data of the roadway was repeated, adjust the original rock mechanical parameters to ensure the accuracy of rock mechanical parameters. On this basis, the mechanism of deformation and instability of surrounding rock in compound roof roadway was revealed. The conclusions obtained from the numerical simulation have a certain degree of agreement with the test range of the loose zone and the deformation of the surrounding rock of the roadway in the previous investigation, which meet the characteristics of deformation and failure of the compound roof roadway under this condition, and have successfully guided the engineering practice to a certain extent. The lack of mutual verification of laboratory tests and numerical simulation results also limits the scope of application of numerical simulation conclusions, which is also the focus of the authors' future research.

This study is aimed at the theoretical and application research of a compound roof roadway engineering under specific conditions. It is impossible to solve the problem of deformation and instability of compound roof roadway under other general conditions. Therefore, the subsequent research should combine a large number of engineering cases, summarize the general rules of

deformation and failure of the compound roof roadway, refine and improve the theoretical calculation model and numerical simulation, which can make the research conclusions more universal. Finally, a unified understanding of the deformation and instability characteristics and stability control of the compound roof roadway was formed.

7. Conclusions

Based on the research background of surrounding rock control of a compound roof roadway in a coal mine in Guizhou Province, China, field investigation, theoretical calculations, numerical simulation, field measurement, and industrial tests were comprehensively used to study the delamination and instability conditions, deformation instability mechanism of compound roof roadway. The control principle and technology of the roadway stability were proposed, and the industrial tests are carried out. The main conclusions are as follows:

(1) The theoretical analysis method was employed to construct the mechanical structure model of the compound roof. Based on the mechanical derivation of the infinite plate, the expressions of the critical load for the separation and instability of the compound roof are obtained. Compound roof abscission testifying was made by including concrete construction geological condition. The result shows that the compound roof of the transportation roadway at the mining face 1603 consisted of two parts, that is, the stratified compound board of mudstone and 5# coal layer, and the stratified compound board made of tonsteins 1 and coal layer 4#, and tonsteins 2 and coal layer 3#. Abscission occurs between these two compound boards.

(2) The numerical simulation method was employed to study the distribution evolution laws of stress, displacement and plastic zone of surrounding rock after the roadway with compound roof is excavated, and to analyze the operating condition of bolt and anchor, which reveals the deformation instability mechanism of roadway with compound roof, that is, as for early stage deformation of roadway, the amount is large, the speed is fast, and the scale is wide; compound roof is vulnerable to abscission and instability, the bearing capacity of the two sides is low due to softness and cracking, the shear failure of side angles and vertex angles weakens the strength of surrounding rock, and the self-bearing capacity of surrounding rock is low; Bolt and anchor bear relatively large tensile force, and the support structure is easy to be broken up.

(3) In the groundwork of the early stage study, stability control principle of the roadway with compound roof was presented, that is, "fast and timely support, strong support of high-strength bolt, and high pre-stress support". Theoretical analysis has also been made. Industrial tests show that the developed stability control technology effectively controls the deformation of a roadway with a compound roof, which ensures the overall stability of the roadway.

Author Contributions: J.B. conceived and designed the research; X.W. performed the numerical simulation and field tests; L.Z. and H.X. provided theoretical guidance in the research process; Y.Y. analyzed the data and wrote the paper. All authors have read and agreed to the published version of the manuscript.

Funding: This research was funded by the National Nature Science Foundation of China grant number No. 51904269 and 51974269, and the Fifth "333 Project" Scientific Research Project of Jiangsu, China in 2019 grant number No. BRA2019236.

Acknowledgments: This research was supported by the National Natural Science Foundation of China (51904269), which is gratefully acknowledged.

Conflicts of Interest: The authors declare no conflict of interest.

References

1. He, F.L.; Yin, D.P.; Yan, H.; Li, K.Q.; Yang, H.Z. The Control of Thick Compound Roof Caving on a Coal Roadway. *Adv. Intell. Syst. Res.* **2010**, *12*, 717–721.
2. Yue, Z.W.; Yang, R.S.; Yan, Z.D.; Wang, G.D.; Wu, B.Y. Numerical Simulation on Support of Roadway with Compound Roof and Large Cross Section. In *International Mining Forum 2010: Mine Safety and Efficient Exploitation Facing Challenge of the 21st Century*; CRC Press: Boca Raton, FL, USA, 2010; pp. 138–143.

3. Su, X.G.; Li, Y.B.; Yang, Y.K. A Research into Extra-thick compound mudstone roof roadway failure mechanism and security control. *Procedia Eng.* **2011**, *26*, 516–523.
4. Hong, Y.; He, F.L.; Yang, H.Z. Study on key supporting techniques of large cross-section roadway in compound mudstone roof. *Rock Mech. Achiev. Ambitions* **2012**, 635–639. [[CrossRef](#)]
5. Song, Z.F.; Lei, J.H.; Wang, X.T.; Xu, X.M.; Xin, X.P. Study on Roadway Parameters of Broken Compound Roof of Gently Inclined Thick Coal Seam. *Energy Procedia* **2012**, *16*, 334–340. [[CrossRef](#)]
6. Zhang, H.Q.; Han, L.S.; Qi, Y.J.; Zhang, Y.F. Stability control mechanism and integral supporting technology of roadways with thick compound roof strata. *Rock Mech. Achiev. Ambitions* **2012**, 709–712. [[CrossRef](#)]
7. Jiang, L.S.; Ma, N.J.; Bai, L.; Li, Y.J.; Zhang, L. Deformation and failure characteristics and roof caving hidden danger classification of roadways compound roof. *J. China Coal Soc.* **2014**, *39*, 1205–1211.
8. Su, X.G.; Song, X.M.; Li, H.C.; Yuan, H.H.; Li, B.K. Study on Coupled Arch-beam Support Structure of Roadway with Extra-thick Soft Compound Roof. *Chin. J. Rock Mech. Eng.* **2014**, *33*, 1828–1836.
9. Fan, D.; Liu, X.; Tan, Y.; Song, S.; Gu, Q.; Yan, L.; Xu, Q. Roof Cutting Parameters Design for Gob-Side Entry in Deep Coal Mine: A Case Study. *Energies* **2019**, *12*, 2032. [[CrossRef](#)]
10. Tai, Y.; Xia, H.; Kuang, T. Failure characteristics and control technology for large-section chamber in compound coal seams—A case study in Tashan Coal Mine. *Energy Sci. Eng.* **2019**. [[CrossRef](#)]
11. Bai, J.B.; Hou, C.J.; Du, M.M.; Ma, D.C. On bolting support of roadway in extremely soft seam of coal mine with complex roof. *Chin. J. Rock Mech. Eng.* **2001**, *20*, 53–56.
12. Wang, H.T.; Zhang, W.M.; Chen, Y.M.; Chen, M.; Yan, K. Semantic Decomposition and Reconstruction of Compound Buildings with Symmetric Roofs from LiDAR Data and Aerial Imagery. *Remote Sens.* **2015**, *7*, 13945–13974. [[CrossRef](#)]
13. Yan, H.; Xu, T.F.; Wang, J. Study on the Deformation Characters of the Coal Roadways with Compound Rock Strata and Water Spraying Roof. Green Power, Materials and Manufacturing Technology and Applications II. *Appl. Mech. Mater.* **2012**, *214*, 287–291. [[CrossRef](#)]
14. Wang, W.-J.; Luo, L.-Q.; Yu, W.-J.; Wu, H.; Qu, Y.-S. Study of dynamic pressure roadway supporting scheme under condition of thick composite roof. *J. Coal Sci. Eng.* **2013**, *19*, 119–125. [[CrossRef](#)]
15. Liang, W.Y. Anchored Structure Technology of Loosen Soft Seam with Big Dip Angle in Compound Roof. In Proceedings of the International Conference on Computer Science and Environmental Engineering, Destech Publications, Beijing, China, 17–18 May 2015; pp. 272–278.
16. Freidin, A.M.; Neverov, A.A.; Neverov, S.A. Geomechanical assessment of compound mining technology with backfilling and caving for thick flat ore bodies. *J. Min. Sci.* **2016**, *52*, 933–942. [[CrossRef](#)]
17. Li, L.; Bai, J.B.; XU, Y.; Xiao, T.Q.; Wang, X.Y.; Zhang, K.X. Research on rock control of roadway with complex roof driven along goaf. *J. Min. Saf. Eng.* **2011**, *28*, 376–383.
18. Li, C.E.; Duan, H.M.; Wang, D.Q. The Application of High Strength Anchor about Compound Roof Support about in Guantun Coal Mine. *Metall. Technol. Mater. II* **2013**, *813*, 281–283. [[CrossRef](#)]
19. Wang, C.; Yang, S.; Li, X.; Yang, D.; Jiang, C. The correlation between dynamic phenomena of boreholes for outburst prediction and outburst risks during coal roadways driving. *Fuel* **2018**, *231*, 307–316. [[CrossRef](#)]
20. Cao, Y.; Lv, X.; Han, G.; Luan, J.; Li, S. Research on Gas-Path Fault-Diagnosis Method of Marine Gas Turbine Based on Exergy Loss and Probabilistic Neural Network. *Energies* **2019**, *12*, 4701. [[CrossRef](#)]
21. Zhang, G.H.; Hao, C.B.; Yu, H.J.; Xu, Y.H. Analysis of Collapse Shape about Mining Gateway under Condition of Compound Roof after Disaster. *J. Heilongjiang Univ. Sci. Technol.* **2014**, *24*. [[CrossRef](#)]
22. Yang, P.; HUA, X.Z.; Yang, K.; PANG, D.D.; Cheng, S.X. Experiment of compound roof deformation characteristics of gob-side retaining entry in deep mine and support measures. *J. Min. Saf. Eng.* **2017**, *34*, 1067–1074.
23. Chang, S.J.; Wi, S.; Cho, H.M.; Jeong, S.-G.; Kim, S. Numerical analysis of phase change materials/wood-plastic composite roof module system for improving thermal performance. *J. Ind. Eng. Chem.* **2020**, *82*, 413–423. [[CrossRef](#)]
24. Wu, D.Y.; Shen, F.J. Quantitative criteria of interlayer separation stability of complex roof in tunnels. *Chin. J. Rock Mech. Eng.* **2014**, *33*, 2040–2046.
25. Zhang, J.W.; Yuan, R.F.; Li, Y.L. Research on surrounding rock control of coal roadway with thick mudstone compound roof. *Chin. J. Rock Mech. Eng.* **2017**, *36*, 152–158. [[CrossRef](#)]

26. Ma, X.G.; He, M.C.; Wang, J.; Gao, Y.B.; Zhu, D.Y.; Liu, Y.X. Mine Strata Pressure Characteristics and Mechanisms in Gob-Side Entry Retention by Roof Cutting under Medium-Thick Coal Seam and Compound Roof Conditions. *Energies* **2018**, *11*, 2539. [[CrossRef](#)]
27. Sun, Y.; Li, G.; Zhang, J.; Qian, D. Experimental and numerical investigation on a novel support system for controlling roadway deformation in underground coal mines. *Energy Sci. Eng.* **2019**, *8*, 490–500. [[CrossRef](#)]
28. Wang, S.R.; He, M.C.; Fan, X.M. Bolt-net supporting technique for a roadway with JS composite soft. *J. Univ. Sci. Technol. B* **2005**, *27*, 390–394.
29. Guo, J.; Feng, G.R.; Wang, P.F.; Qi, T.Y.; Zhang, X.R.; Yan, Y.G. Roof Strata Behavior and Support Resistance Determination for Ultra-Thick Longwall Top Coal Caving Panel: A Case Study of the Tashan Coal Mine. *Energies* **2018**, *11*, 1041. [[CrossRef](#)]
30. Chen, X.; Li, L.; Guo, Z.; Chang, T. Evolution characteristics of spontaneous combustion in three zones of the goaf when using the cutting roof and release pressure technique. *Energy Sci. Eng.* **2019**, *7*, 710–720. [[CrossRef](#)]
31. Jia, H.; Pan, K.; Liu, S.; Peng, B.; Fan, K. Evaluation of the Mechanical Instability of Mining Roadway Overburden: Research and Applications. *Energies* **2019**, *12*, 4265. [[CrossRef](#)]



© 2020 by the authors. Licensee MDPI, Basel, Switzerland. This article is an open access article distributed under the terms and conditions of the Creative Commons Attribution (CC BY) license (<http://creativecommons.org/licenses/by/4.0/>).